Journal of Power Sources 451 (2020) 227740

Contents lists available at ScienceDirect

Journal of Power Sources

journal homepage: www.elsevier.com/locate/jpowsour

Atomic layer deposition synthesized ZnO nanomembranes: A facile route towards stable supercapacitor electrode for high capacitance

Farah Naeem [a,b], Sumayyah Naeem [a,b], Zhe Zhao [b], Gang-qiang Shu [c], Jing Zhang [d,*], Yongfeng Mei [b], Gaoshan Huang [b,**]

[a] State Key Laboratory for Modification of Chemical Fibers and Polymer Material Science and Engineering, Donghua University, Shanghai, 201620, PR China
[b] Department of Materials Science, Fudan University, 220 Handan Road, Shanghai, 200433, PR China
[c] State Key Lab of ASIC and System, Fudan University, 220 Handan Road, Shanghai, 200433, PR China
[d] College of Science, Donghua University, Shanghai, 201620, PR China

HIGHLIGHTS

- ZnO NMs of various thicknesses were successfully synthesized by ALD.
- ZnO NMs electrodes with large capacitance in different electrolytes were obtained.
- The excellent performances were ascribed to effective ion adsorption/desorption.

GRAPHICAL ABSTRACT

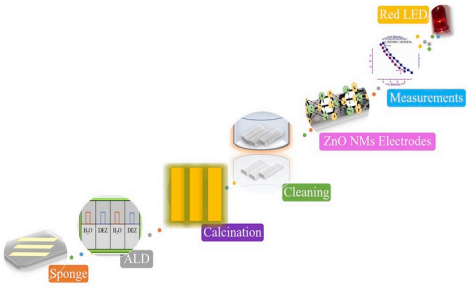

ARTICLE INFO

Keywords:
Atomic layer deposition
ZnO
Nanomembrane
Electrochemical property
Supercapacitor

ABSTRACT

ZnO nanomembranes (NMs) are successfully fabricated by atomic layer deposition for electrochemical supercapacitor applications. The structure and morphology of ZnO NMs are investigated by X-ray diffraction, scanning electron microscopy, X-ray photoelectron spectroscopy, and Raman spectroscopy. In order to prove their potential applications in supercapacitors, the electrochemical performance of ZnO NMs is characterized in the aqueous electrolytes (i.e., KOH, KCl, and Na_2SO_4). Experimental results indicate that 6 M KOH electrolyte is the most promising one, and the largest capacitance of 846 F g^{-1} is achieved in this electrolyte with remarkable stability. In addition, ZnO NM with 100 ALD cycles demonstrates advanced performance in all three aqueous electrolytes, mainly due to the effective ion adsorption/desorption or extraction/insertion in the electrode. The 180-min flashing of a red LED powered by ZnO NMs supercapacitors suggests great potentials of NMs electrodes in practical applications.

* Corresponding author.
** Corresponding author.
E-mail addresses: jingzh@dhu.edu.cn (J. Zhang), gshuang@fudan.edu.cn (G. Huang).

https://doi.org/10.1016/j.jpowsour.2020.227740
Received 2 August 2019; Received in revised form 7 January 2020; Accepted 10 January 2020
Available online 20 January 2020

1. Introduction

Continuous energy demand is a key parameter for modern human society [1]. In order to maintain the living standard, the development of reliable, renewable, clean, and environmentally friendly energy storage and conversion systems with high capacity is required [2]. The non-conventional devices such as batteries, fuel cells, and supercapacitors, are developed to converse chemical energy into electrical energy on the basis of various electrochemical reactions [3]. Among these energy storage devices, supercapacitors are captivated by their high-power density and long lifespan with no memory effect and approximately free of maintenance. In addition, the supercapacitors can function as a bridge for the power-energy difference, filling the gap between conventional capacitors and batteries/fuel cells [4–7]. These properties establish the supercapacitor an approachable energy device to rural areas [3]. Supercapacitors can be used in many devices and occasions such as mobile phones, laptops, digital cameras, hybrid vehicles, and emergency doors [8,9]. The performance of supercapacitor depends on the electrodes, electrolytes, separators, and current collectors [10]. Especially, the electrode material must have high conductivity, large surface area, and good temperature/chemical stability [3,11,12].

Among metal oxides [13–15], zinc oxide (ZnO) has been actively engaged in sensor, transducer, optoelectronics [16], catalyst [17], and energy storage devices [18]. The significant prominence of its electrochemical activity, low tariff as a raw material, and environmental compatibility promote ZnO for active materials of supercapacitor electrode [19]. Unfortunately, the slow faradaic redox kinetics and electron transport capability at high rates affected the performance of the ZnO electrode, leading to low rate capability and poor stability [20]. In this perspective, ZnO nanostructures [13] and ZnO–C (e.g., activated carbon, carbon nanotubes, and graphene) composite structures have been evaluated as electrode materials [21]. For instance, Ranjithkumar et al. [22] embedded the ZnO nanorods on carbon nanotubes to enhance the electrochemical activity. However, the incorporation of carbonaceous materials might lead to relatively lower specific capacitance at high charge/discharge rates and sometimes reduced cycle's life stability can be observed [23,24]. Recently, 2D structures with large surface to volume ratios like thin film structures have attracted tremendous attention for capacitive devices [25]. We consider that the 2D nanomaterials can improve the electron transportation and provide the highly multiple active reaction sites due to short path, and ultra-thin structures may also improve the stability on the basis of their mechanical softness [26,27]. Thus, the application of 2D ZnO nanostructures may pave the way for the future commercialization of ZnO electrode.

Various techniques such as atomic layer deposition (ALD), spray pyrolysis, magnetron sputtering, chemical vapor deposition, sol-gel synthesis, and molecular beam epitaxy have so far been applied to synthesize the 2D ZnO nanostructures [28,29]. Among them, ALD technique has obvious advantages in fabricating nanomembranes (NMs) due to the properties of large surface area, precisely controlled thickness, and highly conformal deposition [30–32]. The surface reaction of two precursors in a repeated manner ensures the deposition of uniform NMs with high quality [33]. Although ALD faces problems like low deposition rate, use of explosive/toxic precursors, high cost of precursors [34], ALD is capable of depositing materials at low temperature on sensitive substrates such as polymers and biological materials which would be damaged at high temperature [35–39]. In addition, ALD controls the chemical and physical natures of ultrathin films/NMs and the surface/interface properties can be tuned [40].

In the present work, in order to fabricate a pristine ZnO NMs supercapacitor electrode, we use ALD of ZnO on polyurethane sponge. We study the influence of the thickness of ZnO NMs which is accurately tuned. Their ultra-thin structures and high surface to volume ratios remarkably enhance the specific capacitance and the cycle stability. Detailed characterization of the ZnO NMs electrodes working in KOH, KCl, and Na_2SO_4 electrolytes is carried out. The results demonstrated that electrochemical performance is significantly affected by the electrolyte. ZnO NMs electrode in KOH electrolyte is superior to that in the KCl electrolyte while it is far superior to that in Na_2SO_4 electrolyte, possibly due to the good affinity of the surface of ZnO NMs in an alkaline aqueous electrolyte. The most favorable achievements such as high capacitance, good rate capability, high energy/power densities, and good cycle stability at high mass loading are obtained in KOH electrolyte by electrode synthesized from ZnO NMs with 100 ALD cycles. The electrode prepared from NMs possesses a high surface area for ion adsorption/desorption and efficiently reduces the diffusion length, and the corresponding excellent performance may have great potential in practical applications.

2. Methods

2.1. ALD of ZnO NMs

In order to grow ZnO NMs with high productivity, here ZnO NMs with various thicknesses (50, 100, and 200 ALD cycles) were deposited on a commercially available polyurethane sponge matrix by using ALD technique. The precursors, i.e., diethylzinc (DEZ) and deionized water (DIW) were delivered into the deposition chamber at 150 °C with the assist of N_2 carrier gas. The precursors used were purchased from J&K Scientific Ltd., China. The flow rate of the carrier gas was 20 sccm. A typical ALD sequence enclosed the following: DEZ pulse (30 ms), waiting time (2 s), N_2 purge (20 s), DIW pulse (20 ms), waiting time (2 s), and N_2 purge (20 s). The polyurethane sponge matrix was then removed after calcination under O_2 atmosphere (600 mL min^{-1}) at 700 °*C* for 3 h. The left ZnO NMs were purified with ethanol and DIW to remove the residual impurities.

2.2. Preparation of ZnO NMs electrode

To develop ZnO NMs electrodes, 90 wt% of active materials (ZnO NMs with 50, 100 and 200 ALD cycles) and 10 wt% of binder (polytetrafluoroethylene, PTFE) were used. A milling process was applied to obtain the homogeneous slurry of ZnO NMs and binder with a small quantity of ethanol. The electrode fabricated by uniformly depositing slurry onto the cleaned Ni foam was degassed at 60 °C for 2 h in a vacuum and finally pressed under 10 MPa pressure. All prepared electrodes were soaked in corresponding electrolytes for 12 h to activate the electrode.

2.3. Microstructural characterizations

The morphologies, crystal structures, compositions, and surface areas of ZnO NMs were inspected by scanning electron microscopy (SEM, Zeiss Sigma)/atomic force microscope (AFM, Dimension Edge, Bruker), X-ray diffraction spectroscopy (XRD, Bruker D8A Advanced XRD with Cu Kα radiation, $\lambda = 1.5405$ Å), Raman spectroscopy (Horiba Scientific Raman spectrometer, $\lambda = 514$ nm), X-ray photoelectron spectroscopy (XPS, PHI 5000C EACA, with C 1s peak at 284.6 eV), and Quantachrome (QUADRA Win analyzer version 5.02) with liquid nitrogen (77 K) absorbate, respectively.

2.4. Electrochemical characterizations

The electrochemical characterizations were carried by Chenhua CHI 660E electrochemical workstation. The electrochemical properties of the ZnO NMs working electrode were recorded on a three-electrode system equipped with Ag/AgCl reference electrode and Pt foil counter electrode. The cyclic voltammetry (CV), chronopotentiometry (CP), and electrochemical impedance spectroscopy (EIS, frequency range of 1–100 kHz with an amplitude of 5 mV) measurements were performed at 25 °C in different electrolytes. The calculation methods of specific

capacitance and energy/power densities are described in Supplementary data.

3. Results and discussion

The rational design of ZnO electrode and corresponding supercapacitor is shown in Fig. 1, and the potential application of powering a red LED is also demonstrated. In order to fabricate ZnO NMs with accurate thicknesses, DEZ and H_2O were used as ALD precursors to conformally coat the polyurethane sponge template at 150 °C as represented in Fig. 1a. Alternative purging of both precursors into the ALD reactor would produce saturated substrate surface and growth of ZnO layer by layer [41,42]:

$$Zn(C_2H_5)_2 + H_2O \rightarrow ZnO + 2C_2H_6 \quad (1)$$

To ensure the separation of ZnO NMs from the sponge template, the coated samples were calcined at 700 °C for 3 h under O_2 atmosphere. The polymer template was changed into CO_2 and ZnO NMs were left [43]. ZnO NMs with different ALD cycles were finally obtained after rinsing in ethanol and DIW to remove organic and inorganic impurities. A large amount of ZnO NMs can be produced by the current template-assisted approach, as shown in Fig. S1a, which demonstrates the potential of current approach for mass production of electrode materials. Fig. S1b exhibits the AFM images of the edges of the ZnO NMs fabricated with different ALD cycles and corresponding thicknesses are derived. Here, the thicknesses are around 8.7 nm, 17.4 nm, and 34.8 nm for ZnO NMs fabricated with 50, 100, and 200 ALD cycles, as demonstrated in Fig. S1b(i). Previous investigations showed that thickness evolution has a strong influence on the ZnO NMs structure [44], and the current ALD-based fabrication route provides a convenient way to study this influence. In addition, as one may expect, the obtained ZnO NMs possess large surface areas. The surface areas measured by the Brunauer-Emmett-Teller technique (Fig. S1c) represents the surface areas of ZnO NMs with 50, 100, and 200 ALD cycles are 92.306, 51.598, and 27.251 $m^2\ g^{-1}$ respectively, due to the thickness tuning. The morphologies of the as-prepared ZnO NMs were studied by SEM and the results are shown in Fig. 1b–d and Figs. S2, S3, and S4. The SEM images in Fig. 1b–d displays that the ZnO NMs with 50, 100, and 200 ALD cycles are obtained in the lateral size of tens of microns. ZnO NMs with 50 ALD cycles in Fig. 1b demonstrates some small holes (red circles). The enhanced flexibility from ultra-thin nature also leads to observed folded edges, ripples, and curls. With the increasing ALD cycles, thicker ZnO NMs become stiffer [45,46], as can be observed in the samples with 100 (Figs. 1c) and 200 (Fig. 1d) ALD cycles. In addition, the additional SEM images in Figs. S2, S3, and S4 illuminate the smooth surfaces of the NMs fabricated with different ALD cycles and the uniformity of the NMs is clearly reflected by the cross sections highlighted by the dashed rectangles therein. The present results demonstrate the ALD with good thickness tuning ability can produce ZnO NMs with different morphologies and the free-standing ultra-thin ZnO NMs fabricated by current approach can possess good flexibility.

The increase of the thickness may also lead to a change in the structural properties of the NMs. Here, the crystallization and phase information of the ZnO NMs were investigated by XRD patterns. Fig. 2a shows XRD patterns of ZnO NMs with different ALD cycles. All the diffraction peaks can be well-indexed to the wurtzite hexagonal phase (space group $P6_3mc$, JCPDS 36–1451) [47], and the strongest peaks are summarized in Table S1. The XRD results prove that the samples are pure ZnO without carbon residue and other detectable impurities [48]. In addition, sharp diffraction peaks indicate the improved crystal quality of the ZnO NMs after high temperature treatment in our experiment [49]. The structure of ZnO NMs were further investigated nondestructively with the help of Raman spectroscopy [50]. Fig. 2b shows the typical Raman spectrum from ZnO NMs with 100 ALD cycles, and Raman mode at 326.5 cm^{-1} from the zone-boundary phonons of 2-E_2(M) can be observed [33]. The dominant peak at 436 cm^{-1} is the characteristic band of the wurtzite phase and linked to the E_2 (high) vibration mode with orientation in the c-axis [51]. No carbon-related Raman peak can be observed, improving the high purity of ZnO NMs fabricated by current approach. In Fig. 2c, XPS spectra from ZnO NMs with 100 ALD cycles are displayed. The results demonstrate the presence of oxygen O 1s peak at 531.6 eV and Zn $2p_{1/2}$ and Zn $2p_{3/2}$ peaks at 1045.8 and

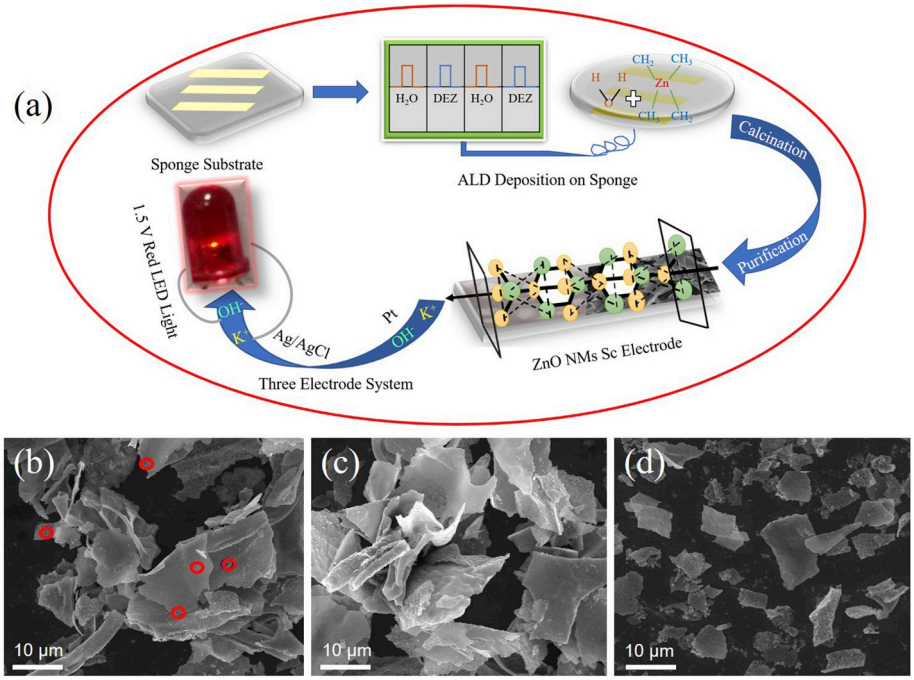

Fig. 1. Design and morphologies of ZnO NMs with various thicknesses. (a) Schematic of the fabrication procedure of ZnO NMs electrode and corresponding supercapacitor. (b-d) SEM images of ZnO NMs with (b) 50, (c) 100, and (d) 200 ALD cycles. The red circles in (b) represent the existence of the holes in ZnO NMs. (For interpretation of the references to colour in this figure legend, the reader is referred to the Web version of this article.)

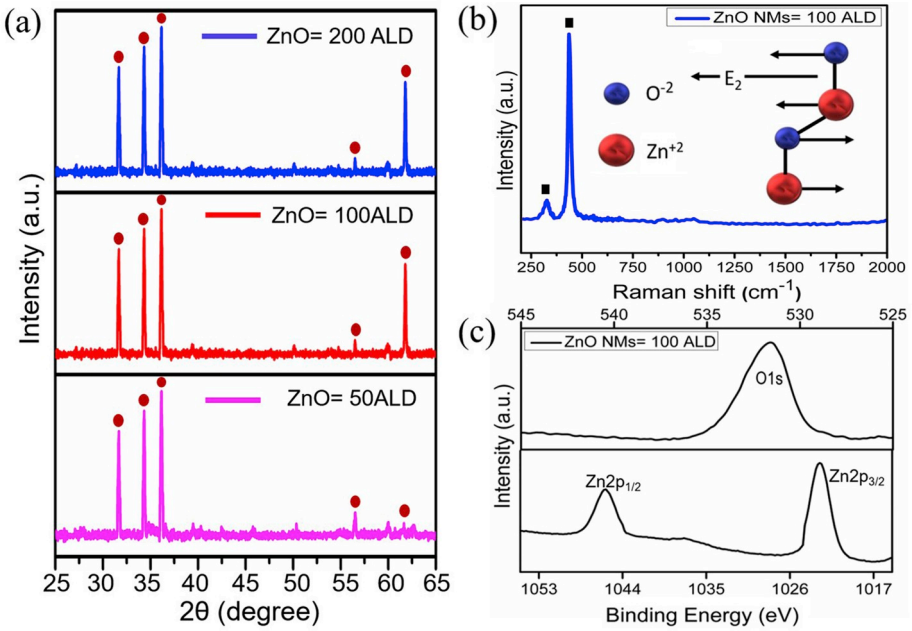

Fig. 2. Structural Characterization of ALD synthesized ZnO NMs: (a) XRD patterns of ZnO NMs with 50, 100, and 200 ALD cycles. The peaks from wurtzite ZnO are marked. (b) Raman spectrum of ZnO NMs with 100 ALD cycles. The inset shows the diagram of E_2 mode. (c) XPS spectrum of ZnO NMs with 100 ALD cycles.

1022.8 eV respectively in wurtzite structure. Moreover, the binding energy of Zn $2p_{3/2}$ peak confirms that the Zn element exists mainly in the form of Zn^{2+} ions [52].

The electrochemical properties of ZnO NMs electrodes were studies in 6 M KOH, 1 M KCl, and 6 M Na_2SO_4 aqueous solutions. Firstly, the performance of ZnO NMs electrodes with high mass loading of ~14 mg cm^{-2} was characterized in 6 M KOH electrolyte. The CV curves of electrode made from ZnO NMs with different ALD cycles were recorded at various scan rates in the potential range of 0–0.6 V (*vs.* Ag/AgCl), and the results are shown in Figs. 3a, S5a, and S6a. All CV profiles present a pair of strong redox peaks, which is undoubtedly capacitive characteristics of the Faradaic redox reaction of pseudocapacitor [53]. The occurrence of surface Faradaic process could be either redox reaction of surface functional groups, or chemical adsorption/desorption [54].

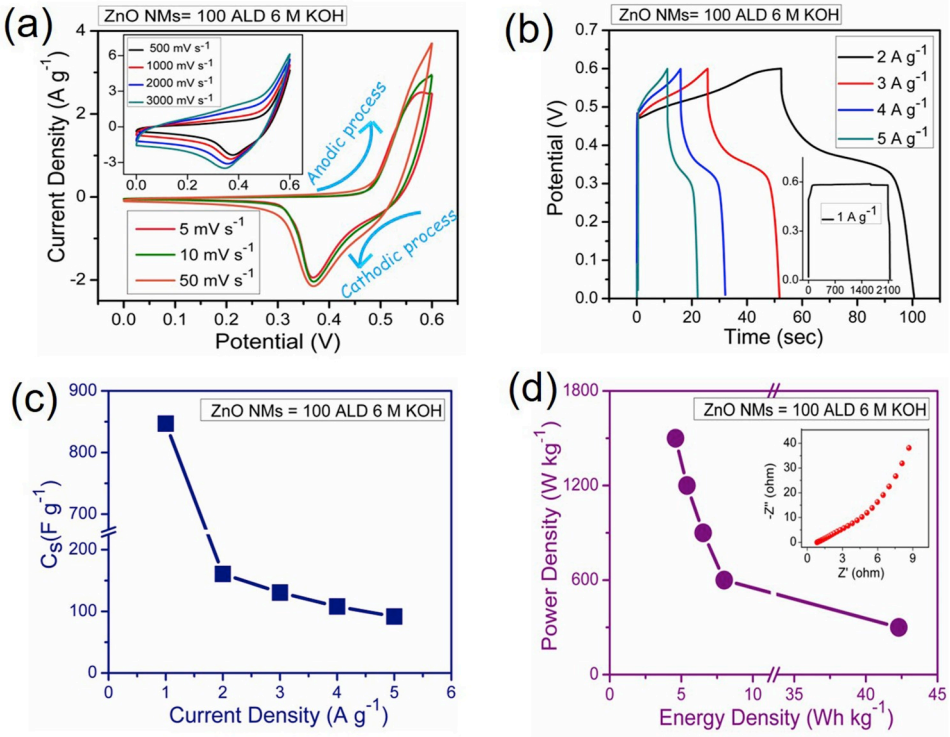

Fig. 3. Electrochemical performance of ZnO NMs with 100 ALD cycles in 6 M KOH aqueous solution. (a) CV profiles at scan rates of 5–3000 mV s^{-1}. The inset shows the CV curves with large scan rates. (b) Charge/discharge profiles at different current densities. (c) Specific capacitance as a function of the current density. (d) Ragone plot of energy and power densities of ZnO NMs electrode. The inset is the Nyquist plot.

Therefore, the possible Faradaic process in our experiment with 6 M KOH electrolyte is described as follows [47,55,56]:

$$ZnO + OH^- \leftrightarrow ZnOOH + e^- \quad (4)$$

$$\text{and } ZnO + K^+ + e^- \leftrightarrow ZnOK. \quad (5)$$

In Fig. 3a, a good redox activity of ZnO NMs with 100 ALD cycles is shown and similar CV curves in the scan rates ranging from 5 to 50 mV s^{-1} can be observed. With further increased scan rate (500–3000 mV s^{-1} in the inset), CV curves demonstrate great rate stability but a diminution of redox peaks is noticeable which is possibly due to the slow surface kinetics/response towards fast sweep rate [57]. At the end of the CV curve, a sharp peak indicates the evolution of oxygen during the electrochemical measurement [58]. We also check the property of thinner ZnO NMs with 50 ALD cycles, and similar redox activities were obtained (Fig. S5a). While for ZnO NMs with 200 ALD cycles (Fig. S6a), limited electrical conductivity at high scan rate is ascribed to the thickness enhancement [59]. In addition, the edge of CV curves in the inset of Fig. S6a with scan rates of 50–500 mV s^{-1} represents a longer diffusion path with dead mass at constant current densities which could be possibly due to the inaccessibility of electrolyte ions [60]. The stabilities of the ZnO NMs in 6 M KOH was examined by CP at various current densities in the potential range of 0–0.6 V, and the results are displayed in Figs. 3b, S5b, and S6b. The appearance of nonlinear CP curves with obvious potential plateaus is highly consistent with Faradaic CV curves. In general, the charging/discharging kinetics includes the electrolyte ions insertion/extraction or adsorption/desorption at the electrolyte/electrode interface. The potential plateau is observed in galvanostatic charge distribution which corresponds to the anodic peak at about 0.6 V in CV behavior. The transformation of the plateau to a higher voltage at higher current densities is the representation of stronger polarization [61]. The specific capacitance of ZnO NM electrode with different NMs thicknesses is shown in Figs. 3c, S5c, and S6c. The calculated gravimetric capacitance at different current densities of electrode fabricated from ZnO NMs with 50, 100 and 200 ALD cycles were 104-27, 846-92, and 197-85 F g^{-1} respectively. The significant capacitance drop of the ZnO NMs electrodes at higher current densities can be attributed to high ion diffusion resistance, slow electrolyte penetration, and poor electrical conductivity [62,63]. Especially, the stack of the NMs in the electrodes hinders efficient electrolyte penetration, leading to the drop of capacitance at high current [53]. It is worth noting that the capacitances of our samples are higher compared with those reported in other ZnO-related nanostructures [55,64,65], proving the superiority of ZnO nanostructure in the form of ALD-produced ultra-thin NMs.

In addition, Fig. 3c illustrates the highest specific capacitance values for ZnO NMs with 100 ALD cycles. The best performance of ZnO NMs with 100 ALD cycles may be connected with suitable ions diffusion, more active sites, and lower interfacial resistance [60]. Obviously, in the case of ZnO NMs with 100 ALD cycles, the flexibility with increased surface area accessibility well-facilitated path of electrons transportation under charging/discharging process [61], and the ascended Faradaic process is closely connected with the higher electron mobility and fast ions diffusion during electrode/electrolyte surface intercalation [66]. On the other hand, the ZnO NMs with 50 ALD cycles are more flexible but overlap, curls, and holes (Figs. 1b and S2) deteriorate the performance. Further, the power densities and energy densities of the ZnO NMs electrodes were also calculated and the energy densities in the ranges of 5-1, 42-5, and 10-4 Wh kg^{-1} were obtained from ZnO NMs with 50, 100, and 200 ALD cycles, respectively, when the power density increases from 300 to 1500 W kg^{-1} (Figs. 3d, S5d, and S6d). The specific capacitance and energy density reduction with increased current density in all samples (see also Tables S2 and S3) can be attributed to the unsustainable active sites in the redox transitions due to the unsatisfactory diffusion rate of the ions [53]. In order to go deeper into the kinetics of the ion insertion/extraction, EIS characterization was carried out. The results in the inset of Fig. 3d reveals a small resistance at low-frequency region for ZnO NMs with 100 ALD cycles, suggesting an easier ions transportation process. On the other hand, the EIS results in the inset of Fig. S5d for ZnO NMs with 50 ALD cycles indicate the unfavorable ions transportation due to the presence of voids, holes, and curls in the thinnest NMs. Besides this, the thick ZnO NMs with 200 ALD cycles also demonstrates large resistance (inset of Fig. S6d), impacting the ion insertion/extraction [67]. The enhanced volume to surface ratio of ZnO NMs with 200 ALD cycles thus reduces the performance remarkably. Overall, the Nyquist plots prove that the electrode made from ZnO NMs with 100 ALD cycles possesses good pseudocapacitive behavior in comparison to those with 50 and 200 ALD cycles.

We also investigated the performances of ZnO NMs electrodes in different electrolytes to check the influence of the electrolyte. For this purpose, electrodes prepared from 100 to 200 ALD cycles were tested in KCl and Na_2SO_4 solutions (see also Supplementary data). The specific capacitances of ZnO NMs electrodes at various current densities were calculated, and the results are exhibited in Fig. 4 and Table S2. The specific capacitances of ZnO NMs with 100 ALD cycles in 1 M KCl solution are 64 to 8 F g^{-1}, corresponding to current densities of 2–5 A g^{-1} (green bars in Fig. 4a, and specific capacitance at 1 A g^{-1} can be found in Table S2). While in 6 M Na_2SO_4 solution, the specific capacitances are 19 to 7 F g^{-1} correspondingly (blue bars in Fig. 4a, and specific capacitance at 1 A g^{-1} can be found in Table S2). For thicker ZnO NMs with 200 ALD cycles, the specific capacitances are 9-3 F g^{-1} in 1 M KCl and 4-2 F g^{-1} in 6 M Na_2SO_4 corresponding to current densities of 1–5 A g^{-1}. Obviously, the performance of the electrode is different in different electrolytes. We consider the reason is mainly due to the size of the ions in the electrolyte. Smaller size of Cl^- ions can easily interact with the surface while larger SO^-_4 ions have less conductivity [68]. And the enhanced performance in KOH solution could be ascribed to the dominate diffusion of OH^- ions which is small and strongly solvated in solution. Furthermore, we compare the performance of supercapacitor electrodes prepared from ALD ZnO NMs with electrodes fabricated from other ZnO-based micro-/nano-structures, and significant performance enhancement is noticeable (see Table S4), proving the advantage of the current ALD-based approach in producing energy storage devices.

The cycling stability characteristic plays an important role in practical applications [69]. Fig. 5a demonstrates the cycle performance of the electrode fabricated from ZnO NMs with 100 ALD cycles. After cycled for 5000 times in 6 M KOH solution, the electrode maintains 89% of its initial capacitance. The good cycle performance in the current case is probably due to the large surface area with good electrolyte accessibility which provides the active path for ions/electrons transportation. In addition, the ALD ZnO NMs are very thin with good flexibility, which may also contribute to the remarkable stability. Fig. 5b demonstrates that two constructed supercapacitors connected in series can flash a red LED light for more than 180 min (Video S1). The initial voltage is observed at 1. 43 V, as shown in Fig. 5b. The voltage increases to ~1.5 V within 15 min and is maintained for 45 min indicating good stability. After that, the small voltage drops to ~1.45 V occurs and the LED is on for 180 min. The results demonstrate that ALD synthesized ZnO NMs could be a promising material for practical energy storage applications.

Supplementary data related to this article can be found at https://doi.org/10.1016/j.jpowsour.2020.227740.

4. Conclusion

A large amount of free-standing ZnO NMs were synthesized with ALD technique and explored as supercapacitor electrodes. The performance of the electrodes made from thin ZnO NMs with different thicknesses were investigated. Especially, electrode fabricated from ZnO NMs with 100 ALD cycles demonstrates a high specific capacitance of 846 to 92 F g^{-1} in 6 M KOH, 465 to 8 F g^{-1} in 1 M KCl, and 65 to 7 F g^{-1} in Na_2SO_4 electrolyte, corresponding to current density of 1–5 A g^{-1}. The corresponding cycling test in 6 M KOH electrolyte exhibits good stability and

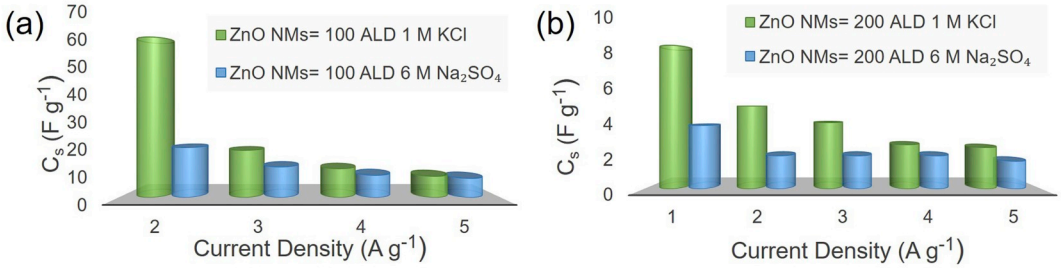

Fig. 4. Electrochemical performance of ZnO NMs with 100 and 200 ALD cycles in 1 M KCl and 6 M Na_2SO_4 aqueous solutions. (a) Specific capacitances of ZnO NMs with 100 ALD cycles at different current densities. (b) Specific capacitances of ZnO NMs with 200 ALD cycles at different current densities.

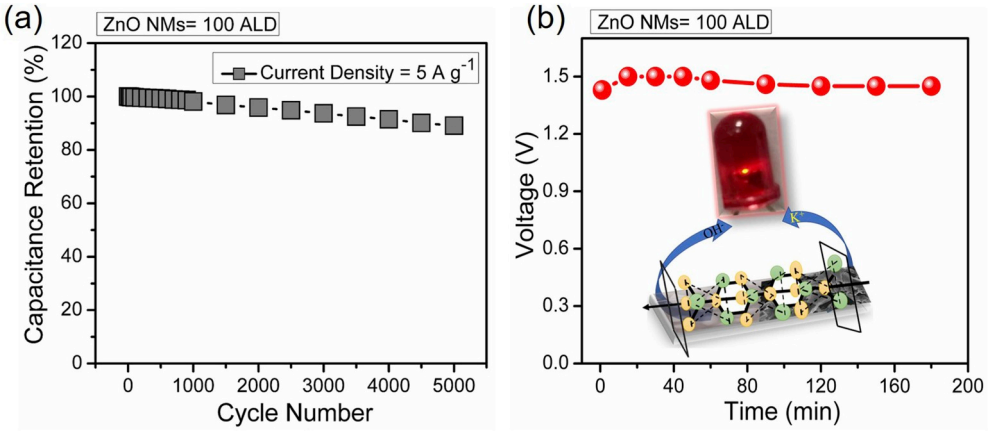

Fig. 5. (a) Cycle performance of the electrode prepared from ZnO NMs with 100 ALD cycles. The electrolyte used is 6 M KOH solution. (b) Potential stability of the supercapacitor made by ZnO NMs with 100 ALD cycles.

the electrode maintains 89% of its initial capacitance after 5000 cycles. The excellent performance of ZnO NMs electrode is ascribed to the large surface excess and enhanced ion intercalation/deintercalation, which provides the fast ions transportation into ZnO NMs structure. The flexibility of the thin NMs is considered to contribute to the enhanced stability. The characterization of the electrodes in different electrolytes indicates the K^+ and OH^- ions are good exchangers and the best performance is obtained in KOH electrolyte. The fabricated pseudocapacitor device can flash a red LED with potential constancy for 180 min. The ZnO NMs provides a new option in the development of energy storage device to achieve a goal of high energy and power densities with appropriate material-electrolyte compatibility selection.

Availability of data and materials

The datasets generated during and/or analyzed during the current study are available from the corresponding author on request.

Authors' contributions

FN carried out the experiment, analyzed the data, and wrote the manuscript. SN helped in analyzing the data and manuscript reading. ZZ helped in results discussion. GS helped in characterization. JZ, YFM, and GSH provided the research directions and revised the manuscript. All authors read and approved the final manuscript.

Declaration of competing interest

The authors declare that they have no known competing financial interests or personal relationships that could have appeared to influence the work reported in this paper.

Acknowledgement

This work was supported by the Natural Science Foundation of China (Nos. 51961145108 and 61975035), the Science and Technology Commission of Shanghai Municipality (Nos. 19XD1400600 and 17JC1401700), and the National Key R&D Program of China (No. 2017YFE0112000).

Appendix A. Supplementary data

Supplementary data to this article can be found online at https://doi.org/10.1016/j.jpowsour.2020.227740.

References

[1] J. Yan, Q. Wang, T. Wei, Z. Fan, Adv. Energy Mater. 4 (2014) 1300816–1300859.
[2] A.S. Arico, P. Bruce, B. Scrosati, J.M. Tarascon, W. Van Schalkwijk, Nat. Mater. 4 (2005) 366–377.
[3] Poonam, K. Sharma, A. Arora, S.K. Tripathi, J. Energy Storage 21 (2019) 801–825.
[4] B.M. Sánchez, Y. Gogotsi, Adv. Mater. 28 (2016) 6104–6135.
[5] G.S. Huang, Y.F. Mei, Small 14 (2018) 1703665–1703688.
[6] C. Liu, F. Li, L.-P. Ma, H.-M. Cheng, Adv. Mater. 22 (2010) E28–E62.
[7] L.L. Zhang, X.S. Zhao, Chem. Soc. Rev. 38 (2009) 2520–2531.
[8] A. Balducci, R. Dugas, P. Taberna, P. Simon, D. Plee, M. Mastragostino, S. Passerini, J. Power Sources 165 (2007) 922–927.
[9] C. Largeot, C. Portet, J. Chmiola, P. Taberna, Y. Gogotsi, P. Simon, J. Am. Chem. Soc. 130 (2008) 2730–2731.
[10] S. Kandalkar, D. Dhawale, C. Kim, C. Lokhande, Synthetic Met 160 (2010) 1299–1302.
[11] P. Simon, Y. Gogotsi, Nat. Mater. 7 (2008) 845–854.
[12] P. Liu, J. Liu, S. Cheng, W. Cai, F. Yu, Y. Zhang, P. Wu, M. Liu, Chem. Eng. J. 328 (2017) 1–10.
[13] M.S. Yadav, N. Singh, A. Kumar, J. Mater. Sci. Mater. Electron. 29 (2018) 6853–6869.
[14] F. Wang, X. Wu, X. Yuan, Z. Liu, Y. Zhang, L. Fu, Y. Zhu, Q. Zhou, Y. Wu, W. Huang, Chem. Soc. Rev. 46 (2017) 6816–6854.

[15] L. L. Zhang, Z. Lei, J. Zhang, X. Tian, X. S. Zhao. Encyclopedia of Inorganic and Bioinorganic Chemistry, Online © 2011 John Wiley & Sons, Ltd. DOI: 10.1002/9781119951438.eibc0464.
[16] S.J. Lim, S. Kwon, H. Kim, Thin Solid Films 516 (2008) 1523–1528.
[17] C. Chen, Z. Hu, J. Ren, S. Zhang, Z. Wang, Z.Y. Yuan, ChemCatChem 11 (2019) 868–877.
[18] F. Wang, J.H. Seo, G. Luo, M.B. Starr, Z. Li, D. Geng, X. Yin, S. Wang, D.G. Fraser, D. Morgan, Z. Ma, X. Wang, Nat. Commun. 7 (2016) 10444–10450.
[19] X. Zhao, X. Liu, F. Li, M. Huang, J. Mater. Sci. 55 (2020) 2482–2491.
[20] C.H. Kim, B.-H. Kim, J. Power Sources 274 (2015) 512–520.
[21] W. Raza, F. Ali, N. Raza, Y. Luo, K.-H. Kim, J. Yang, S. Kumar, A. Mehmood, E. E. Kwon, Nano Energy 52 (2018) 441–473.
[22] R. Ranjithkumar, S.E. Arasi, S. Sudhahar, N. Nallamuthu, P. Devendran, P. Lakshmanan, M.K. Kumar, Physica B 568 (2019) 51–59.
[23] V. Augustyn, P. Simon, B. Dunn, Energy Environ. Sci. 7 (2014) 1597–1614.
[24] X. Zhao, B.M. Sánchez, P.J. Dobson, P.S. Grant, Nanoscale 3 (2011) 839–855.
[25] Z. Tong, Y. Ji, Q. Tian, W. Ouyang, Chem. Commun. 55 (2019) 9128–9131.
[26] X. Peng, L. Peng, C. Wu, Y. Xie, Chem. Soc. Rev. 43 (2014) 3303–3323.
[27] M. Beidaghi, Y. Gogotsi, Energy Environ. Sci. 7 (2014) 867–884.
[28] H.Z. Huang, Y. Song, Y.D. Feng, Z. Sun, Q.X. Sun, X.X. Liu, ACS Nano 12 (2018) 3557–3567.
[29] T. Tynell, M. Karppinen, Semicond. Sci. Technol. 29 (2014), 043001-043016.
[30] A.S. Asundi, J.A. Raiford, S.F. Bent, ACS Energy Lett 4 (2019) 908–925.
[31] T. Wang, Z. Luo, C. Li, J. Gong. Chem. Soc. Rev. 43 (2014) 7469–7484.
[32] R.L. Puurunen, Chem. Vap. Depos. 9 (2003) 249–257.
[33] S.D. Elliott, Semicond. Sci. Technol. 27 (2012), 074008.
[34] P.O. Oviroh, R. Akbarzadeh, D. Pan, R.A.M. Coetzee, T.-C. Jen, Sci. Technol. Adv. Mater. 20 (2019) 465–496.
[35] X. Meng, X.-Q. Yang, X. Sun, Adv. Mater. 24 (2012) 3589–3615.
[36] J.D. Ferguson, A.W. Weimer, S.M. George, Chem. Mater. 16 (2004) 5602–5609.
[37] J. Park, T.-H. Jung, J.-H. Lee, H.-S. Kim, J.-S. Park. Ceram. Inter. 41 (2015) 1839–1845.
[38] J. Malm, E. Sahramo, J. Perälä, T. Sajavaara, M. Karppinen, Thin Solid Films 519 (2011) 5319–5322.
[39] E. Guziewicz, M. Godlewski, L. Wachnicki, T.A. Krajewski, G. Luka, S. Gieraltowska, R. Jakiela, A. Stonert, W. Lisowski, M. Krawczyk, J.W. Sobczak, A. Jablonski, Semicond. Sci. Technol. 27 (2012), 074011.
[40] L.S. Aravinda, K.K. Nagaraja, H.S. Nagaraja, K.U. Bhat, B.R. Bhat, Electrochim. Acta 95 (2013) 119–124.
[41] S.Y. Pung, K.L. Choy, X. Hou, C. Shan, Nanotechnology 19 (2008) 435609–435616.
[42] T. Singh, T. Lehnen, T. Leuninga, D. Sahu, S. Mathur, Appl. Surf. Sci. 289 (2014) 27–32.
[43] Y.T. Zhao, G.S. Huang, D.R. Wang, Y. Ma, Z.Y. Fan, Z.H. Bao, Y.F. Mei, J. Mater. Chem. 6 (2018) 22870–22878.
[44] A.A. Chaaya, R. Viter, M. Bechelany, Z. Alute, D. Erts, A. Zalesskaya, K. Kovalevskis, V. Rouessac, V. Smyntyna, P. Miele, Beilstein J. Nanotechnol. 4 (2013) 690–698.
[45] Y.T. Zhao, G.S. Huang, Y.L. Li, R. Edy, P.B. Gao, H. Tang, Z.H. Bao, Y.F. Mei, J. Mater. Chem. 6 (2018) 7227–7235.
[46] R.L. Puurunen, J. Appl. Phys. 97 (2005) 121301–121354.
[47] X. Xiao, B. Han, G. Chen, L. Wang, Y. Wang, Sci. Rep. 7 (2017) 40167–40179.
[48] Y.T. Prabhu, K.V. Rao, V.S.S. Kumar, B.S. Kumari, Adv. Nanoparticles 2 (2013) 45–50.
[49] Y. Aouna, B. Benhaouac, S. Benramached, B. Gasmi, Optik 126 (2015) 5407–5411.
[50] C. Geng, Y. Jiang, Y. Yao, X. Meng, J.A. Zapien, C.S. Lee, Y. Lifshitz, S.T. Lee, Adv. Funct. Mater. 14 (2004) 589–594.
[51] K.A. Alim, V.A. Fonoberov, M. Shamsa, A.A. Balandin, J. Appl. Phys. 97 (2005) 124313–124317.
[52] I.G. Morozov, O.V. Belousova, D. Ortega, M.K. Mafina, M.V. Kuznetcov, J. Alloy. Comp. 633 (2015) 237–245.
[53] F. Naeem, S. Naeem, Y.T. Zhao, D.R. Wang, J. Zhang, Y.F. Mei, G.S. Huang, Nanoscale Res. Lett. 14 (2019) 92–101.
[54] J. Wang, S.P. Feng, Y. Yang, N.Y. Hau, M. Munro, E.F. Yang, G. Chen, Nano Lett. 15 (2015) 5784–5790.
[55] M. Saranya, R. Ramachandran, F. Wang, J. Sci. Adv. Mater. Dev. 1 (2016) 454–460.
[56] X. He, J.E. Yoo, M.H. Lee, J. Bae, Nanotechnology 28 (2017) 245402–245413.
[57] S. Ratha, A.K. Samantara, K.K. Singha, A.S. Gangan, B. Chakraborty, B.K. Jena, C. S. Rout, ACS Appl. Mater. Interfaces 9 (2017) 9640–9653.
[58] Z.S. Wu, W. Ren, D.W. Wang, F. Li, B. Liu, H.M. Cheng, ACS Nano 4 (2010) 5835–5842.
[59] H.C. Han, C.W. Chong, S.B. Wang, D. Heh, C.A. Tseng, Y.F. Huang, S. Chattopadhyay, K.H. Chen, C.F. Lin, J.H. Lee, L.C. Chen, Nano Lett. 13 (2013) 1422–1428.
[60] L. Qu, Y. Zhao, A.M. Khan, C. Han, K.M. Hercule, M. Yan, X. Liu, W. Chen, D. Wang, Z. Cai, W. Xu, K. Zhao, X. Zheng, L. Mai, Nano Lett. 15 (2015) 2037–2044.
[61] Z. Xing, Q. Chi, X. Ren, C. Ge, A.H. Qusti, A.M. Asiri, A.O. Al-Youbi, X. Sun, J. Power Sources 245 (2014) 463–467.
[62] L.L. Jiang, L.Z. Sheng, C.L. Long, Z.J. Fan, Nano Energy 11 (2015) 471–480.
[63] S.L. Liu, J.S. Xu, J.X. Zhu, Y.Q. Chang, H.G. Wang, Z.C. Liu, Y. Xu, C. Zhang, T. X. Liu, J. Mater. Chem. 5 (2017) 19997–20004.
[64] H. Mahajan, J. Bae, K. Yun, J. Alloy. Comp. 758 (2018) 131–139.
[65] D. Kalpana, K.S. Omkumar, S.S. Kumar, N.G. Renganathan, Electrchim. Acta. 52 (2006) 1309–1316.
[66] X. Wang, J. Hao, Y. Su, F. Liu, J. An, J. Lian. J. Mater. Chem. A 4 (2016) 12929–12939.
[67] K.R. Nandanapalli, D. Mudusu, ACS Appl. Nano Mater. 1 (2018) 4083–4091.
[68] J.H. Chae, G.Z. Chen, Particuology 15 (2014) 9–17.
[69] X. Xia, D. Chao, Z. Fan, C. Guan, X. Cao, H. Zhang, H.J. Fan, Nano Lett. 14 (2014) 1651–1658.